An investigation of infrared spectral features related to the presence of lithium in micas,

East Kemptville tin deposit, Nova Scotia

By
Travis G. Kendall

A Thesis Submitted to
Saint Mary's University, Halifax, Nova Scotia
in Partial Fulfillment of the Requirements for
a Bachelor of Science, Honours Degree in Geology.

April 28th, 2017, Halifax, Nova Scotia

Approved: Dr. Jacob Hanley
Associate Professor

Date: April 28, 2017

An investigation of infrared spectral features related to the presence of lithium in micas, East Kemptville tin deposit, Nova Scotia

by Travis G. Kendall

Abstract

Lithium is an important commodity in the rapidly growing rechargeable battery industry and it is unclear whether future Li-demand will outgrow current supply. As such, it is important that the groundwork for exploration be ready in the event of a Li shortage. One possible source is within Li-micas in Sn-greisen deposits. The use of infrared spectroscopy, a cheap and portable technique, for Li-quantification within greisen-style mineralogy was explored. To do this, recreation of the 915 cm^{-1} signature, which was found to decrease in intensity as a function of octahedral Li occupancy after treatment of muscovite with molten $LiNO_3$ (White et al., 1961) was explored. Recreation of this feature was unsuccessful, which is likely due to a lack of empty octahedral positions to accommodate Li^+ cations pre-treatment. The orientation of samples during analyses, both parallel and perpendicular to mica cleavage was found to have no effect on the wave number position of absorption features. Intensities o individual absorption features were found to vary as a function of sample thickness. In addition to this, the absorption features of 6 mica samples with varying Li concentration were compared. Absorption near 1411 and 2200 cm^{-1} were found to be shifted to higher wave numbers in samples with the highest Li, reflecting the replacement of octahedral Al by Li.

April 28th, 2017

Acknowledgements

I would like to thank Dr. Jacob Hanley for a number of things. Thank you for continuously making the subject of geology fascinating throughout my degree, and encouraging me to take on more than the minimum amount of work required. No one else could have taken on these tasks. Thank you for placing your faith in my ability to complete this project. Lastly, thank you for the guidance, and the knowledge you've instilled in me over the years. Catherine Sedge, thank you for your support throughout this project. You set the framework for this study, and provided technical advice and moral support throughout my work. Dr. Tony Barresi, thank you for your tutelage on the basics of infrared spectroscopy and the instrument I used throughout the study. Members of the Royal Ontario Museum (ROM), thank you for providing the samples required to perform this study. Last, but certainly not least, I would like to thank my parents, Barb and Guy Kendall, for supporting me throughout my degree, both financially and emotionally. I could not have accomplished any of this without you.

Table of Contents

List Of Figures

List of Tables

1.0 Introduction

Magmatic-hydrothermal greisens (a type of endoskarn) form during hydrothermal alteration of granitoid rocks by high temperature fluids that can be enriched in ore-forming metals and other elements exsolved from fluid-saturated felsic magmas. Several of these ore-forming elements concentrate in greisens producing economic deposits (Eugster, 1985), such as at the East Kemptville Sn-Cu-Zn deposit, in SW Nova Scotia, Canada. Ore-forming elements such as Zn, Cu, Sn, W, Mo, Nb, Ta and Li can concentrate in tri- and di-octahedral micas through minor structural substitutions (e.g., biotite and muscovite, respectively) and also in major concentrations in some end-member micas (e.g., polylithionite, trilithionite) in greisenized granites and pegmatites (Eugster, 1985). For example, at the East Kemptville deposit, Nova Scotia, Li-bearing sheet silicates (Li-muscovite, polylithionite and zinnwaldite; Sedge 2015) occur in abundance within the intrusive rocks and peripheral to the intrusions where they come into contact with metasediments.

Lithium has a wide range of industrial uses including ceramics and glass, continuous casting mold flux powders, air treatment, polymer production, and primary aluminum production (Jaskula, 2016). Figure 1 shows the relative importance of these industrial uses. Currently, the use of Li in rechargeable batteries for mobile devices, electric cars, electric tools and home power-grid storage accounts for the biggest portion of the demand. As rechargeable Li-batteries are becoming more common, there is an increase in Li demand (Jaskula, 2016). With the projected increase in Li-demand, it is unclear whether future Li-demand will outgrow current supply (Gruber et al., 2011; Kesler et al., 2012). Furthermore, the majority of Li reserves are concentrated in just a few countries. With 78% of Li reserves

concentrated in China, Australia and Argentina, it is important for smaller contributors to secure more resources to meet future demand. Figure 2 shows the global distribution of Li reserves. Due to this increase in Li demand, and the need for geographic diversification of Li resources, including the possibility of recovering Li from these micas rather than more traditional host phase (eg; spodumene) is being considered (Allen, 2015).

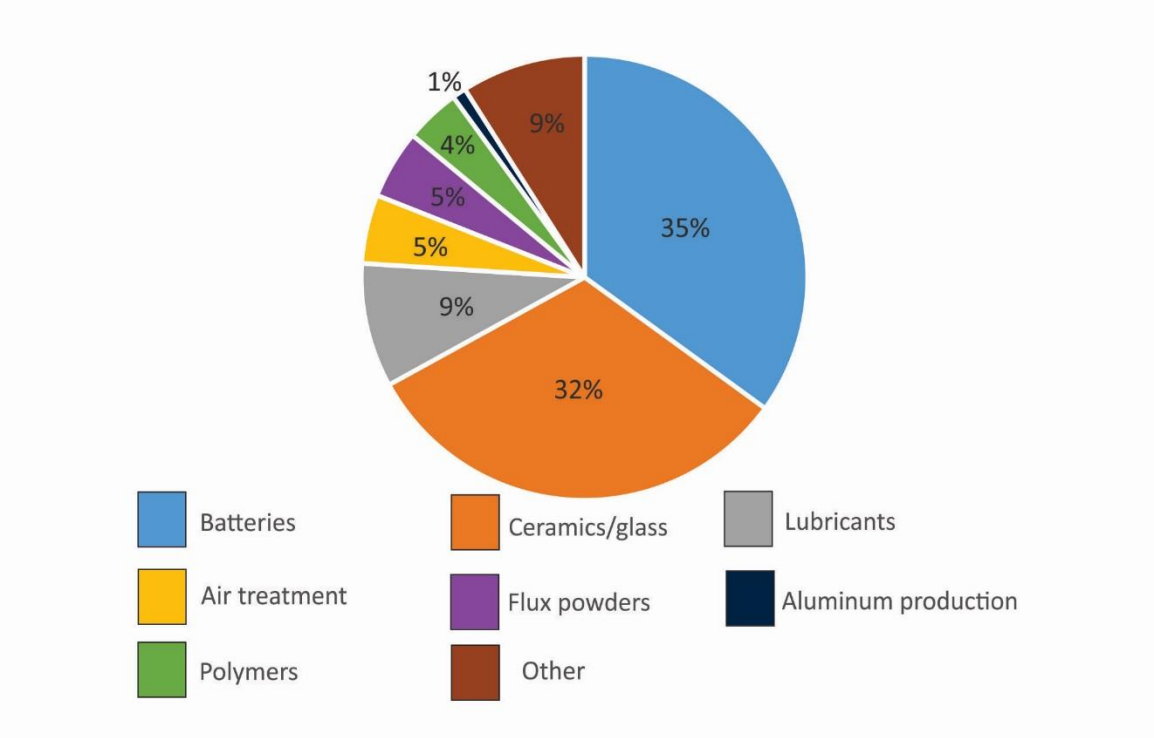

Figure 1: Global industrial consumption of Li as of 2015 showing its importance in rechargeable batteries, ceramic and glass production and other applications (Jaskula, 2016).

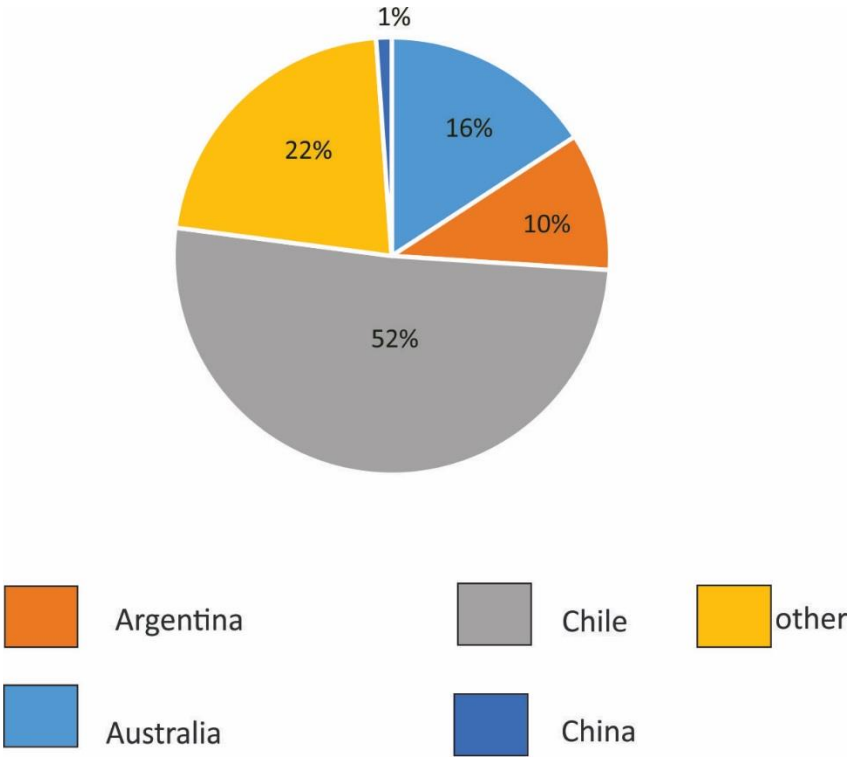

Figure 2: Global distribution of lithium reserves. 78 % of reserves are concentrated in just 3 countries; China, Australia and Argentina (Jaskula, 2016).

While Li-containing minerals exist in Sn-W deposits, analytical tools available to identify them through the detection and quantification of Li, or recognition of their characteristic spectral features, are limited. Techniques that enable identification of Li-bearing minerals include secondary ion mass spectrometry (SIMS; e.g., Henderson et al., 1989), laser ablation inductively-coupled ion mass spectrometry (LA-ICP-MS; e.g., Bea et al., 1994) and Raman spectroscopy (e.g., Robert et al., 1989). More traditional methods of mineral and bulk rock analysis are limited by a range of issues both fundamental to the measurement technique and also inherent to the element's properties. For example, electron microprobe is a preferred method for geologists when analyzing minerals in-situ, but it cannot be used to quantify Li due to low yields for characteristic X-ray lines, uncertainties in mass absorption coefficients, limited available reference standards, and detector window composition restricting the minimum energy of characteristic X-rays emitted from the sample that can be analyzed (Tischendorf et al., 1999). Indirect methods of Li quantification via microprobe have been attempted by analyzing/quantifying elements that can be detected, and quantified, and that correlate (through structural associations) with Li abundance in micas (Tindle & Webb, 1990; Tischendorf et al., 1997). Since LA-ICPMS, SIMS, Raman spectroscopy, and even electron microprobe analyses are relatively expensive to access (and in some cases not available widely), and non portable they are impractical for many geologists who wish to get information about sample composition rapidly to inform exploration efforts, and/or during field campaigns (Tischendorf et al., 1999).

Whereas SIMS and LA-ICPMS yield isotope measurements and absolute concentrations of Li in minerals, Robert et al. (1989) used Raman spectroscopy to analyze

synthetic solid solutions of micas and related variations of spectral features to differences in the amount of Li present. Specifically, they analyzed mixtures including phlogopite[$KMg_3(Si_3Al)O_{10}(F,OH)_2$]-polylithionite[$KLi_2Al(Si_4O_{10})(F,OH)_2$], phlogopite[$KMg_3(Si_3Al)O_{10}(F,OH)_2$]-trilithionite [$K(Li_{1.5}Al1._5)(AlSi_3O10)(F,OH)_2$], and phlogopite[$KMg_3(Si_3Al)O_{10}(F,OH)_2$]-taeniolite[$KLiMg_2Si_4O_{10}F_2$] and attributed shifts in the absorption related to the OH-stretching region to the varying abundance of Li in the micas. They observed that OH groups bonded to Mg_2Li or Li_2Al produced a peak in the 3755-3740 cm^{-1} range. Bonding of OH to Mg_3 or AlMgLi produced a peak in the 3740 to 3715 cm^{-1} range. Bonding with Mg_2Al or Al_2Li was linked to peaks produced in the < 3700 cm^{-1} range. A peak at 3595 cm^{-1} was linked to the presence of 2Mg and a lack of Li. So, while Raman spectroscopy provides spectral data that can aid in the positive identification of Li minerals as well as assist with structural interpretation of these species, it is still limited in that it is not-portable and therefore cannot be used for field work.

Infrared (IR) spectroscopy is unique in that it is a technology that allows for rapid analysis (i.e., 10 spectra per second) via a field-portable spectrometer that is comparatively inexpensive, allowing for in-situ mineral characterization in the field. Characterization of Li-bearing micas has been attempted using IR in the past. Most work of this nature focused on the OH-stretching range (3550-3750 cm-1). For example, Jorgensen (1964) described the absorption bands for polylithionite, lepidolite, and zinnwaldite. Polythionite was characterized by the presence of a strong band (3535 cm^{-1}), and two weaker bands (3730 and 3710 cm^{-1}). Lepidolite was characterized by one strong band (3588 cm^{-1}) and two weaker bands (3485 and 3680 cm^{-1}). Zinnwaldite was characterized by one strong band

(3575 cm^{-1}), one intermediate strength band (3480 cm^{-1}) and two weaker bands (3665 and 3645 cm^{-1}). These findings are summarized in Figure 3.

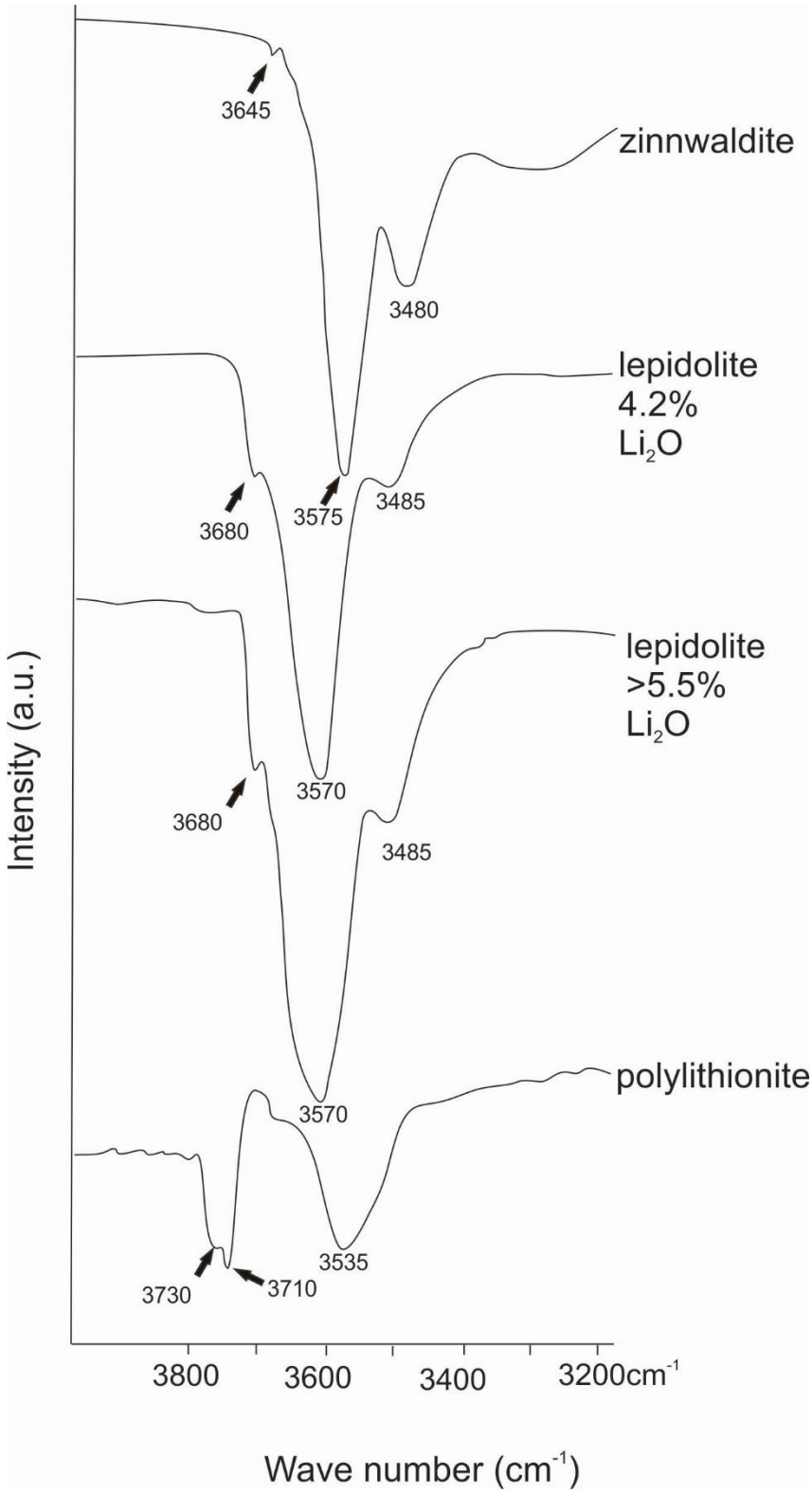

Figure 3: Summary of high-wave number absorption features in various Li-micas modified from Jørgensen (1964). Arrows identify the position of characteristic bands for each mineral.

Unfortunately, many field spectrometers are limited to the mid-IR range, preventing their ability to detect Li-related features at >2500 cm^{-1}. Furthermore, features attributed to Li in lower wave-numbers are not well understood. There is some evidence to suggest that the migration of Li into octahedral sites within muscovite decreases absorption at 915 cm^{-1} (White et al., 1961).

This thesis attempts to characterize the IR spectral features of octahedrally-coordinated Li in micas containing variable amounts of Li. To do this, dioctahedral and trioctahedral mica species with varying Li abundance were been analyzed with an ASD (Analytical Spectral Devices) Terraspec® 4 IR spectrometer manufactured in Boulder, Colorado. The same samples were then analyzed for bulk Li content by LA-ICPMS. By comparing the spectra of these samples to their Li content, the study attempted to define what spectral features, if any, differ as Li concentrations vary. Drill core from the East Kemptville deposit was also analyzed to see if any Li-related spectral features could be detected in natural samples. If a characteristic spectral feature (or features) could be recognized, it would allow for a field-based approach for the detection of high Li intervals in drill core, hand samples or mining faces in the East Kemptville deposit.

The study also investigated the role of mica grain orientation on the resulting IR spectra. Because these elements are contained within octahedral sites and, the study attempted to find IR signatures of these elements by comparing resultant spectra when the probe was oriented parallel, and perpendicular to the cleavage direction. another purpose of this was to increase the surface area of exposed octahedral layers, with the intent of detecting a signature related to octahedral cations. If there are absorption features unique to the mineral when viewed in the octahedral orientation, they may originate from octahedral cations.

A final goal of the study was to reproduce the experimental work of White et al. (1961), who attributed an absorption feature at 915 cm^{-1} to the lack of Li in empty octahedral sites of muscovite. In their study, this feature was no longer present in samples after treatment of muscovite with molten $LiNO_3$. If the feature loses intensity as a function of Li octahedral occupancy, it may be useful in quantification of Li in micas using IR spectroscopy.

2.0 Geological setting

2.1 Exploration history and deposit background

In the 1970s, the East Kemptville Sn-Cu-Zn deposit was discovered 55 km northeast of Yarmouth, Nova Scotia, and quickly became North America's only primary tin deposit. The 56 Mt deposit was large enough and close enough to the surface for open pit mining (Halter, 1996). mining began in 1982 and continued for 10 years until the mine was forced to close due to declining Sn price. Before closure, the deposit was processing 9000 tonne/day ore which produced 4000 tons Sn/year, making it a historically significant producer for Canada (Kontak & Dostal, 1992).

Though East Kemptville is historically significant, there has been recent interest in its current and future economic potential. Avalon Advanced Materials Inc. (formerly Avalon Rare Metals Inc.) has recently purchased mineral rights to the property in response to increasing and sustained Sn prices. The property still contains a large amount of stock-piled ore which is available for processing and new drilling has delineated geological resources within 3-4 mineralized zones that were not known or exploited previously. Furthermore, the deposit is accessible by local roadways. The accessibility of the deposit coupled with the presence of previously unprocessed ore stock pile, newly discovered

mineralized zones, and existing open pit infrastructure contribute to confidence in its economic viability in today's Sn market.

2.2 Regional geology

From 405-390 Ma, the Meguma Terrane accreted onto North America by colliding into the Avalon terrane forming the Cobequid-Chedabucto fault system along the terrane junction (Muecke et al., 1988). This event positioned the southern half of what is now Nova Scotia onto the eastern North American margin. Of those rock types within that part of Nova Scotia, the South Mountain Batholith (SMB) largely consists of granitoid rocks, and is the largest intrusive sequence of such rocks in the entire Appalachians. The granitoids are hosted within metasedimentary rocks of the Meguma Terrane and formed at ~ 370 Ma by the emplacement of partial melts derived from Avalonia granulite facies rocks at depth (Kontak & Chatterjee, 1992).

2.3 Local geology

Many of the SMB granitoid rocks within the Meguma terrane host mineral deposits. The East Kemptville deposit is an example of a Sn-In-Cu-Zn vein-stockwork type deposit (Sinclair, 1996). The deposit is associated with the 360-370 Ma old granitic Davis Lake Pluton (DLP), emplaced during the latest stages of accretion of the Meguma terrane (Kontak & Chatterjee, 1992). The main mineralization occurs near the contact between the DLP and the surrounding Meguma metawackes (metaturbidites). The DLP is a leucogranite which formed via fractionation of the SMB and occurs at the SW termination of the SMB (Kontak & Chatterjee, 1992; Figure 4). Though hydrothermal alteration is most intense near the contact, it extends into both the Meguma metawackes and the DLP (Figure

5). Fluid-rock interaction has led to this alteration and is expressed as massive and layered greisens in the DLP-Meguma contact region (Kontak, 1990). A large NE-SW oriented concentration of faults and fractures comprises the East Kemptville-East Dalhousie fault zone, which runs through the DLP (Kontak et al., 1986). The alteration is spatially associated with these faults and fractures, which are thought to have acted as conduits for the hydrothermal fluids responsible for alteration and mineralization (Halter et al., 1996). It is around this fault zone that the open pit was constructed for mining of the Sn ore.

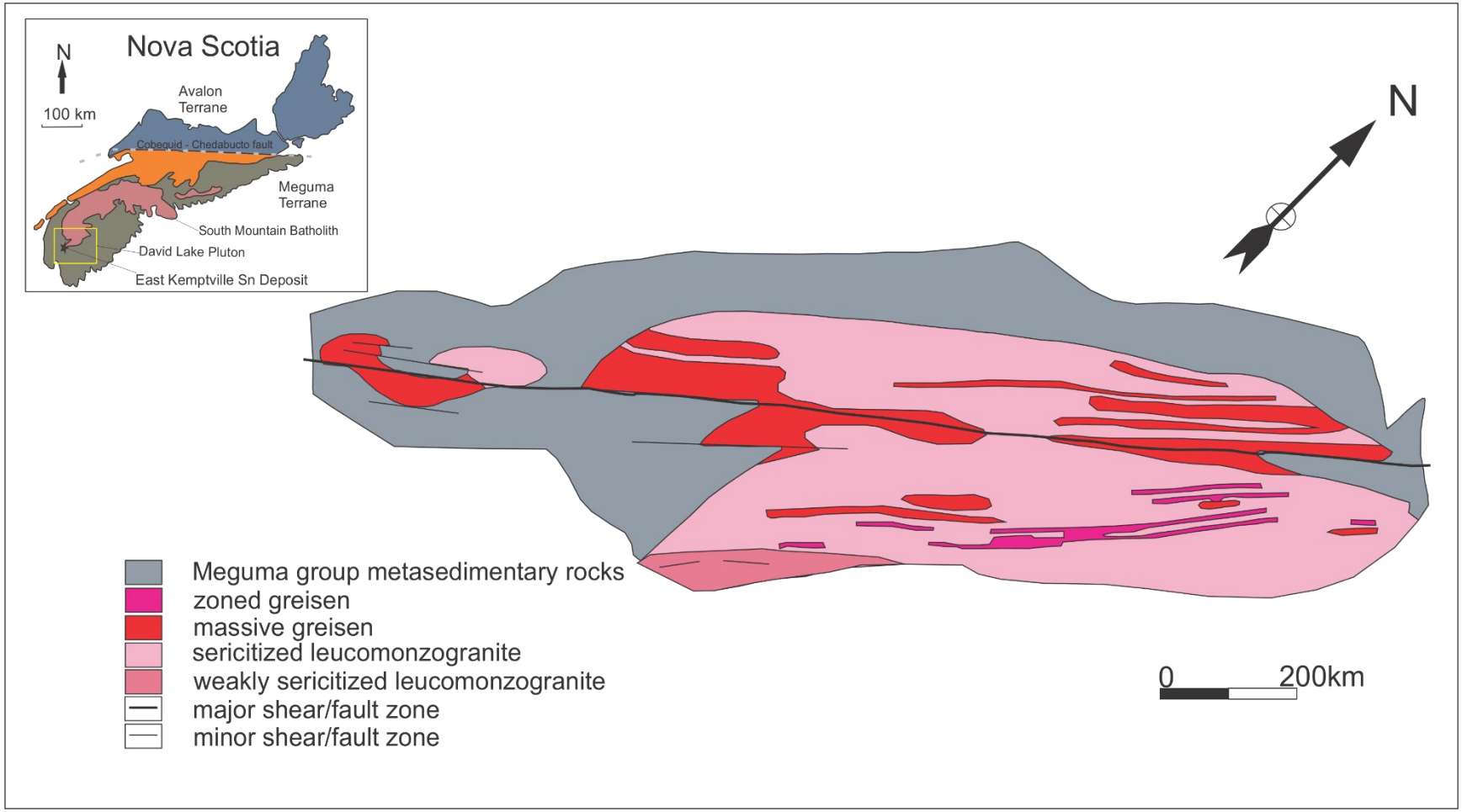

Figure 4: Plan-view of the East Kemptville open pit shows massive greisen veins within the Davis Lake leucomonzogranite. Alteration is spatially associated with the NE-SW oriented Cobequid-Chedabucto fault modified from Halter et al. (1996).

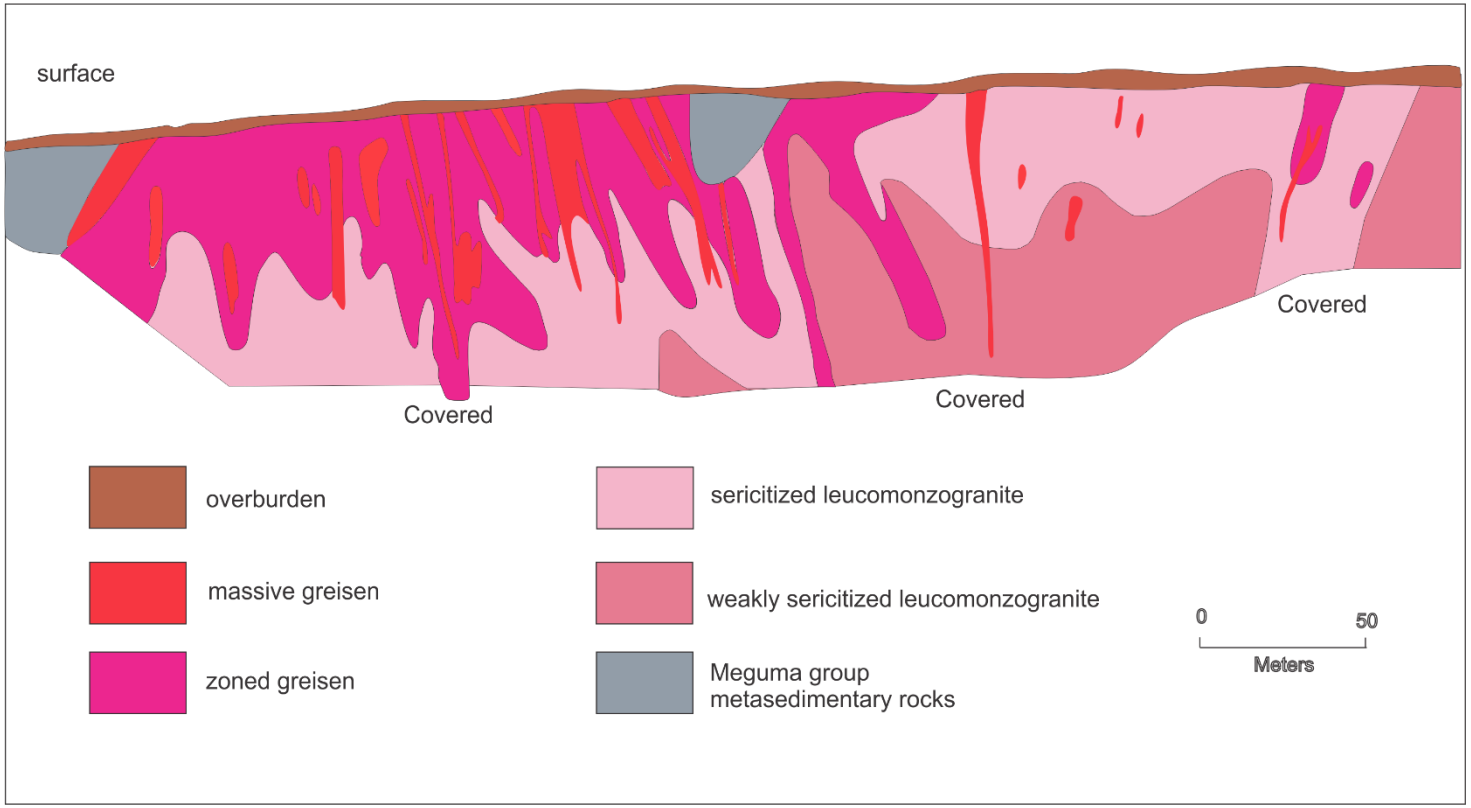

Figure 5: Excavated section through mineralized contact between the Davis Lake pluton and Meguma metawackes provides cross-section showing greisenized veins extending into complex stockwork of greisen alteration. Image not spatially related to previous Figure 4 Image modified from Sinclair (1996).

2.4 Deposit scale characteristics

Kontak (1990) described the mineralogy and geochemistry of the East Kemptville leucomonzogranite in detail. The intrusive leucomonzogranite has been described as homogenous, medium-grained, and equigranular with a dome-like structure due to its doubly plunging attitude. Conversely, the host rocks have been described as hornfelsed, antiformal metasediments (Kontak, 1990).

The study by Kontak (1990) showed that the granite has elevated concentrations of incompatible elements including Rb, Cs, Ga, Li, Sn and Nb and is depleted concentrations of compatible elements including Ba, Th, V, Sc, Hf, Cr, Ni. The study also showed the main minerals found within the leucomonzogranite include quartz, plagioclase, potassium-feldspar, muscovite and topaz with accessory biotite, zircon, monazite, and that the main Sn ore mineral is cassiterite. Sedge (2015) later described the Li mineralogy in the intrusion, the contact and the host metasediments. The main Li-minerals are zinnwaldite and muscovite with minor tourmaline in the intrusion, phlogopite, zinnwaldite, and muscovite in the metasedimentary rocks, and zinnwaldite, muscovite and tourmaline in the contact zone.

2.5 Fluid-rock interaction and alteration history

Greisenization is an essential process for the formation of Sn-W deposits (Sinclair, 1996). In general, this style of mineralization requires hydrothermal alteration of granitic rocks by internally derived, acidic, saline, F-bearing magmatic fluid (Halter et al., 1996). This fluid transports a variety of incompatible trace elements including ore metals that are derived from exsolved volatiles from the magmas, and in some cases, elements derived

through interaction of fluids with country rocks. These metals are transported to the depositional site and will precipitate out of solution to form ore minerals like cassiterite content (Eugster, 1985), and accessory minerals including hydrothermal micas that may contain elevated Li.

At the East Kemptville deposit, the alteration history has been deconstructed using the major and trace element chemistry determined at set distances from the most heavily altered rocks outward (Halter et al., 1996). In the zones proximal to the heaviest zones of alteration, muscovite converted to topaz and quartz by the reaction:

$$4.50\ KAl_2(AlSi_3O_{10})(F,OH)_2 + 5.99Al(OH)_3 + 1.92FeCl^+ + 1.07ZnCl_2 + 17.07HF + 3.30HCl + 10.78H_2S + 3.59O_2 + 1.29Cl^- \rightleftharpoons 16.09SiO_2 + 14.59Al_2SiO_4(F,OH)_2 + 4.86FeS_2 + 1.07(Zn,Fe)S + 9.12KCL + .14NaCl + 33.10H_2O \quad (1)$$

In the areas distal from the heaviest zones of alteration albite was replaced by muscovite in the greisenization reaction:

$$8.42\ NaAlSi_3O_8 + 2.36\ KCl_{aq} + .96\ FeCl^+ + .6\ ZnCl_2 + 1.5HF + 1.22\ HCl + .99\ H_2S + 1.47\ H_2O + .19O_2 + .96Cl^- \rightleftharpoons 1.75\ SiO_2 + .27Al_2SiO_4(F,OH)_2 + 1.2KAl_2(AlSi_3O_{10})(F,OH)_2 + .6(Zn,Fe)S + .2FeS_2 + 2.52Al(OH)_3 + 6.70Nacl_{aq} \quad (2)$$

Halter et al. (1996) explains that fluids entered complex fractures in the host rock leading to the first reaction, and later travelled distally through microfractures to participate in the second reaction. This multi-stage process created the complex vein-stockwork structure of the ore zones depicted in Figure 5.

2.6 Lithium as a possible secondary commodity

The East Kemptville deposit is considered a primary Sn deposit. However, there has recently been interest in Li as a secondary commodity (Allen, 2015) that occurs within the waste Meguma rock adjacent to mineralization and in the DLP-Meguma contact region. Interestingly, these Li enrichments do not correlate with Sn enrichment and so were formed by some other process, or Li was decoupled from Sn in terms of transport and precipitation mechanisms (Sedge, 2015). The source of Li may also have been be different than the Sn (Sedge, 2015).

3.0 Analytical Methods

Five standard samples from the muscovite-lepidolite group were obtained from the Royal Ontario Museum. An additional muscovite standard from an unknown location was also used (Table 1). The samples were chosen based on their varying mineral classification and Li concentrations from sample to sample. To observe IR spectroscopic changes related Li content, two drill core samples of increasing Li content from the contact between the Davis Lake pluton and the Meguma metwackes were also analyzed.

Table 1: Table of samples used for infrared studies of micas containing Li. Samples were chosen based on their varying species from the tri and dioctahedral family of micas and therefore, the expectation that their Li contents are different from sample to sample.

Label	Mass (g)	Mineral Class	Locality
m10000	25	muscovite	unknown
m6317	0.42	muscovite	Auburn, Maine
m55285	0.11	polylithionite	Narsaq, Greenland
m31893	0.65	lepidolite	Tordal, Norway
m29059	4.99	lepidolite	Minas Gerais, Brazil
m23374	1.65	lepidolite	Brown Derby Pegmatite, Colorado

3.1 Infrared spectroscopy (IR)

Samples were analyzed on a Terraspec 4 Hi-Res mineral spectrometer equipped with a 6.5 W, 10mm ASD Hi-bright contact probe. This was used to create spectrograms for each of the 6 standards as well as 2 selected core samples from the SD14129800 drill hole. All readings were taken at room temperature. Spectra in the VNIR (350-1000 cm^{-1}), SWIR1 (1000-1800 cm^{-1}), and SWIR2 (1800-2500 cm^{-1}) ranges were analyzed. Spectra were analyzed using ASD RS^3 software that comes with the spectrometer. Specifications of the instrument are shown in Table 2.

Table 2: Summary of specifications of and analytical conditions for the Terraspec® 4 infrared spectrometer.

Specification	Value
Spectral Resolution	3nm at 700 nm 6nm at 1400 nm 6nm at 2100 nm
Sampling interval	1.4nm from 350-1000nm 2nm from 1000-2500nm
Scan time	30s
Scans/second	10

Calibration was done in accordance with the ASD Terraspec® user manual for each sample reading. First, the instrument was set to do a 10-spectrum averaging and the instrument was optimized to the "Spectralon" white reference. This allows the software to create a reference line for which all spectral responses of samples can be compared. The spectrum averaging during referencing was set to 60 readings for white reference and dark current. To reduce noise (background energy from the instrument itself) in spectra, all actual unknown sample measurements were collected with 100 spectrums averaged.

To reduce contamination during calibration, the Spectralon standard was cleaned with compressed air before each calibration. To control contamination during sample measurements, samples were placed on clean paper before each reading and samples were stored in separate plastic bags between readings.

To produce clean, readable spectrographs, raw data was processed using viewspecpro software. To ensure continuity in relative reflectance between the different wave-ranges of the probes, a splice correction was performed for each spectrograph using the viewspecpro software.

3.1.2 Orientation

To determine the influence of mica grain orientation on spectra, readings were taken of sample m10000 at multiple orientations. First, spectra were collected from the flat lying tetrahedral orientation. Then, the sample was cut into strips and stacked together to produce enough surface area for the probe to measure. Finally, a second reading was taken of the stacked samples from the octahedral orientation (Figure 3). Spectra for both orientations were used to create a spectrograph for later comparison.

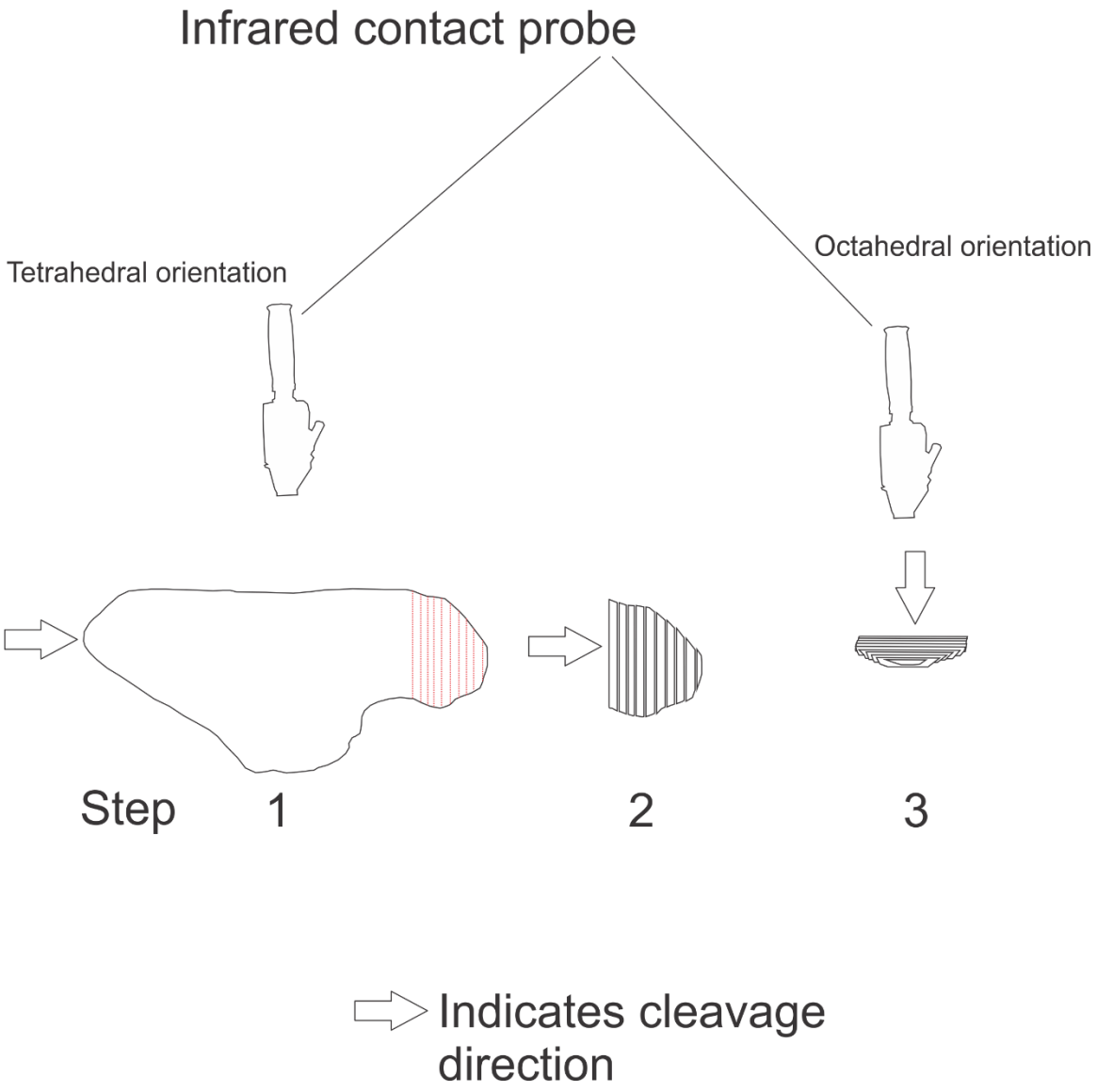
Infrared contact probe
Tetrahedral orientation
Octahedral orientation
Step 1
2
3
Indicates cleavage direction

Figure 6 (previous page): Experimental procedure to determine the effect of orientation on infrared spectra. 1) readings are taken from the flat-lying tetrahedral orientation 2) sections are cut to increase surface area of the octahedral layers 3) readings are taken from the stacked muscovite sections in order to focus on the octahedral layers.

3.1.3 Treatment with lithium nitrate ($LiNO_3$)

To investigate the findings of White et al. (1961), a similar protocol from the original paper was followed (Figure 7). Two pieces of sample m10000 were placed in separate alumina crucibles. Powdered $LiNO_3$ was packed into one crucible, labeled "treated", while the other, labeled "control", was not filled with $LiNO_3$. Both the treated and control crucibles were put into a muffle furnace (KSL-1700X; MTI Corporation, California) and heated to 300C (2 hour ramp) and held at that temperature for specific durations (72 and 240 hours). After each run duration, the samples were quenched in air to ambient conditions within 20 minutes by removing the crucibles from the furnace. They were then rinsed with tap water for 15 minutes. Infrared spectroscopic measurements were then taken from the treated and control sample.

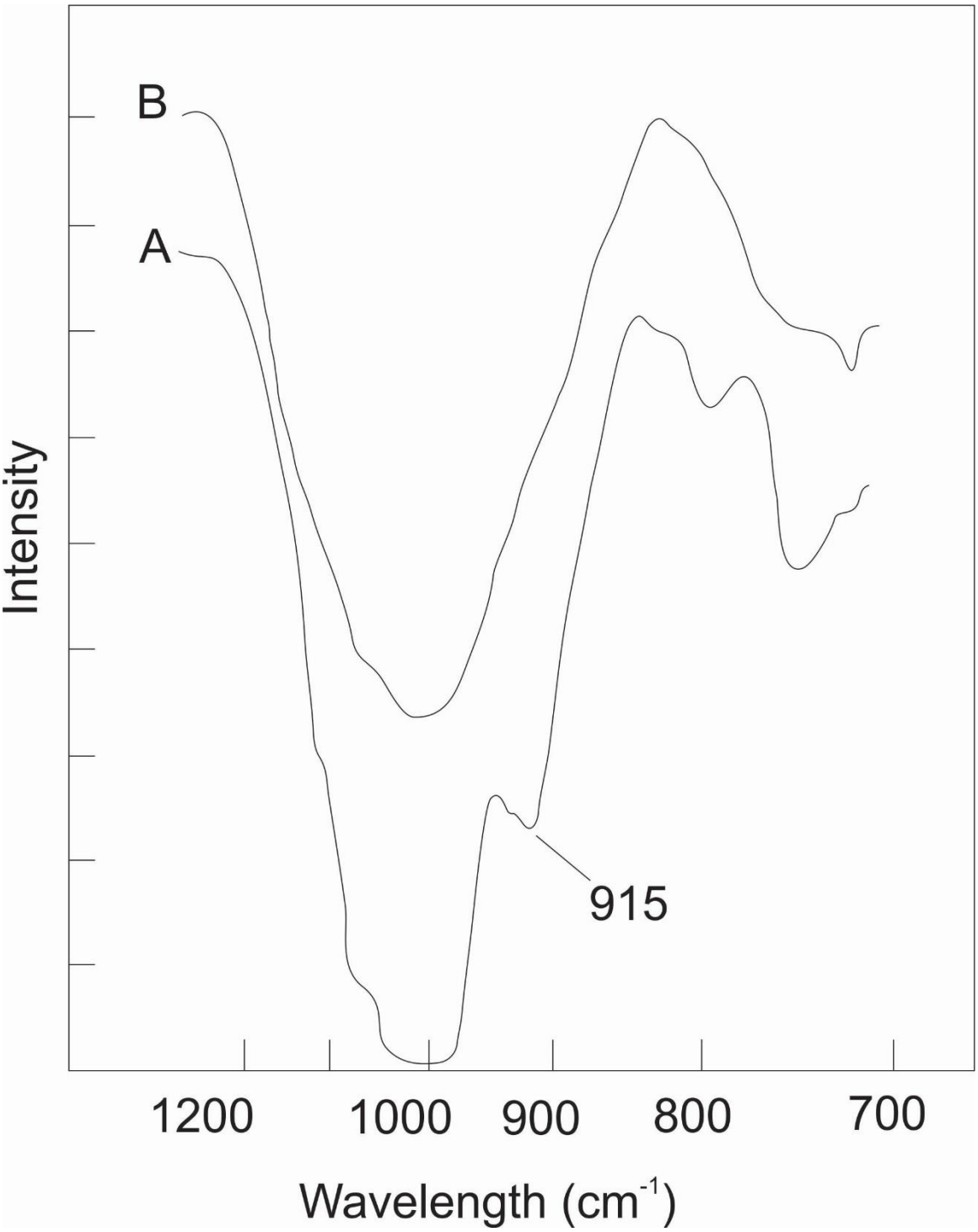

Figure 7: Model infrared spectra of A) untreated muscovite and B) the same muscovite after being bathed with molten $LiNO_3$ at 300C for 480 hours. Modified from White et al. (1961).

3.2 Scanning electron microscopy (SEM)

A TESCAN MIRA 3 LMU Variable Pressure Schottky Field Emission Scanning Electron Microscope (FESEM) at Saint Mary's University was used for Al_2O_3 determination to be used as an internal standard for LA-ICP-MS calibration. A tungsten filament was used to bombard the sample with electrons, creating a back scattered image (BSE). This required a small fragment of each mica which was coated in an ultrathin carbon-polish and mounted on a thin section before analysis. The SEM also uses energy dispersive spectrometry (EDS) to allow chemical analysis of each spot selected, with data output in element and oxide percent. The SEM has a best resolution of 1.2 nm at 30kV. This study used an accelerating voltage of 20kV for all measurements. It is equipped with an INCA X-max 80 mm^2 silicon-drift detector (SDD) EDS system and INCA software was used for data collection.

3.3 Laser Ablation Inductively Coupled Plasma Mass Spectrometry (LA-ICP-MS)

The 6 standard samples were analyzed for selected major and trace elements including Li by a Resonetics S-155-LR 193nm Excimer laser ablation system coupled to an Agilent 7700x quadrupole ICP-MS at the University of New Brunswick in Fredericton, New Brunswick. Spots were analyzed on individual grains with a 33 micron laser. Data were quantified using the Iolite Software with the Al_2O_3 weight % from SEM-EDS analyses for internal standardization.

4.0 Results

4.1 Infrared spectroscopy (IR)

To identify IR absorption features caused by Li in micas, 6 mica samples and 2 drill core samples of from the contact of the East Kemptville deposit were analyzed with a Terraspec® 4 infrared spectrometer. Figure 8 shows the position and relative intensity of

absorption features for each of the 6 standard samples. All absorption features for the 6 mica samples are summarized in Table 3. Figure 9 shows the position and relative intensity of absorption features for the two drill core samples. There are 5 main observations:

1) An absorption band is observed from 1411-1418cm^{-1} in all standards. This feature is less pronounced in samples m1000, m55285 and to some extent, m295059. This feature occurs at a higher wave number (1436 cm^{-1}) in M55285.
2) In natural samples, an absorption band near 1411-1418 cm^{-1} occurs at higher wave number (1420 cm^{-1}) in the sample with the highest Li content (r334063)
3) An absorption band is observed from 2193 to 2202cm^{-1} in all standards with the exception of m55285. This feature occurs at higher wave-numbers (2210cm^{-1}) in m55285.
4) An absorption band from 563 to 584cm^{-1} was observed in all samples apart from M55285.
5) An absorption band is observed from 404 to 405 cm^{-1} in m6317 and m295059. None of the other samples show absorption near this range.

Table 3: Summary of IR absorption features of 6 Li-micas.

Sample	Feature #	Wavelength (cm^{-1})	Intensity	Description	Description	Mineral	Mean Li (ppm)
m55285	1	1195	2676	SiO_2 stretching	Beran, 2002	polylithionite	32375
	2	1366	624	-	-		
	3	1438	1375	OH bending	Clark 1999		
	4	1720	1403	-	-		
	5	1916	1915	-	-		
	6	2094	1059	-	-		
	7	2266	1857	-	-		
	8	2304	1863	OH vibration	Clark 1999		
m295059	1	405	1478	SiO_2 bending	Beran, 2002	lepidolite	28158
	2	563	2647	SiO_2 bending	Beran, 2002		
	3	836	1340	SiO_2 stretching	Beran, 2002		
	4	1411	4769	OH bending	Clark 1999		
	5	1477	1844	-	-		
	6	1923	2128	-	-		
	7	2106	1557	-	-		
	8	2202	4127	Al-OH vibration	Duke 1994		
	9	2350	1629	OH vibration	Clark 1999		
m31893	1	572	1034	SiO_2 bending	Beran, 2002	muscovite	26837
	2	1415	1046	OH bending	Clark 1999		
	3	2209	3442	Al-OH vibration	Duke 1994		
	4	2289	1240	OH vibration	Clark 1999		
	5	2336-2362	1623	OH vibration	Clark 1999		
m10000	1	564	1241	SiO_2 bending	Beran, 2002	muscovite	54
	2	1418	1265	OH bending	Clark 1999		
	3	1926	1515	-	-		
	4	2094	682	-	-		
	5	2209	1251	Al-OH vibration	Duke 1994		
m23374	1	567	1240	SiO_2 bending	Beran, 2002	lepidolite	28447
	2	965	-	SiO_2 stretching	Beran, 2002		
	3	1410	4586	OH bending	Clark 1999		
	4	1721	1400	-	-		
	5	1914	1284	-	-		
	6	2196	3802	Al-OH vibration	Duke 1994		
	7	2341-2440	1676	OH vibration	Clark 1999		
m6317	1	404	2205	SiO_2 bending	Beran, 2002	muscovite	1958
	2	584	-				
	3	910	2181	SiO_2 stretching	Beran, 2002		
	4	963	2086	SiO_2 stretching	Beran, 2002		
	5	1193-1199	1680	SiO_2 stretching	Beran, 2002		
	6	1411	6571	OH bending	Clark 1999		
	7	2193	4305	Al-OH vibration	Duke 1994		
	8	2336	1810	OH vibration	Clark 1999		

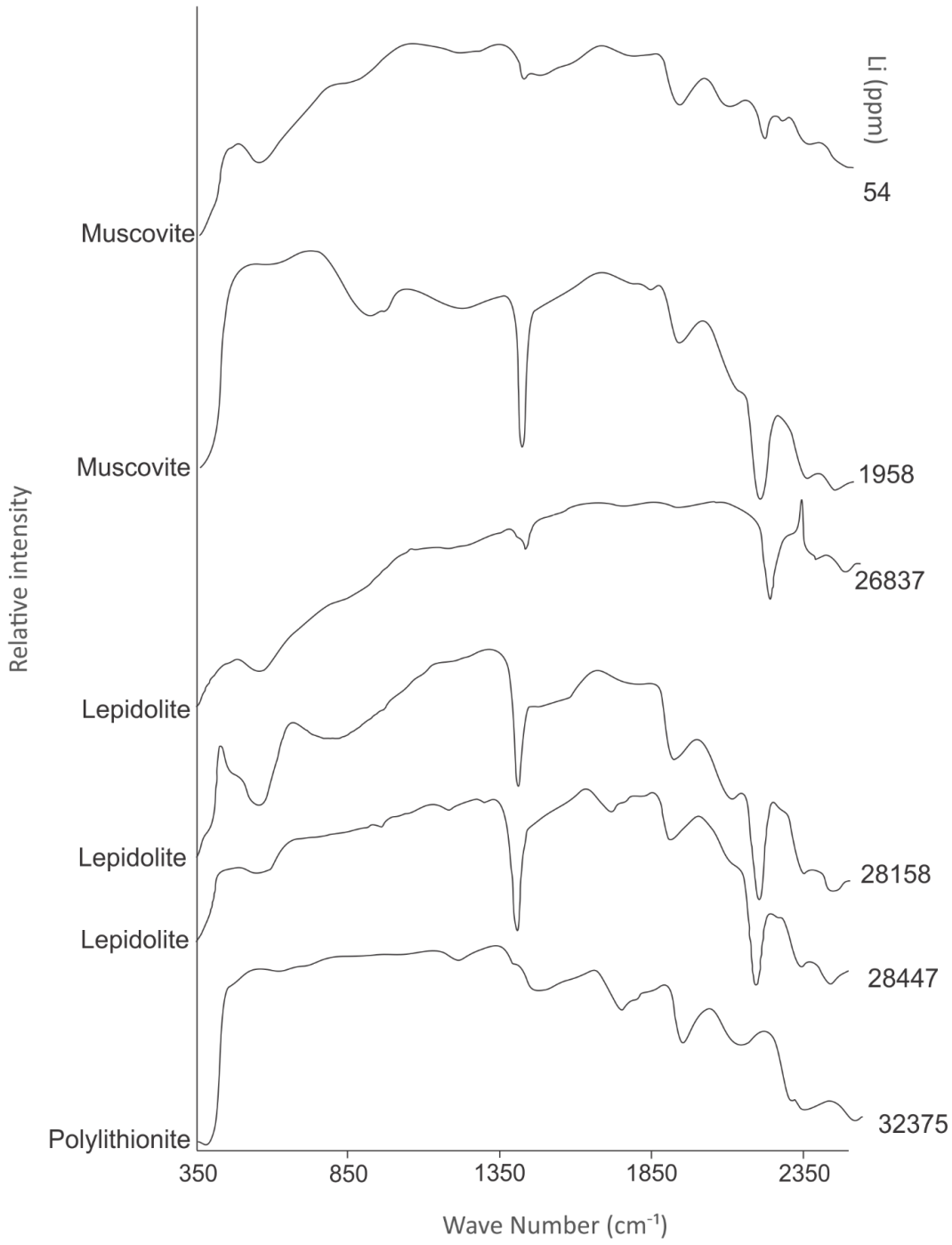
Li (ppm)
54
Muscovite
Muscovite
1958
26837
Lepidolite
Lepidolite
28158
Lepidolite
28447
32375
Polylithionite
Relative intensity
350
850
1350
1850
2350
Wave Number (cm-1)

Figure 8: Infrared spectra of 6 standard samples of increasing Li concentration: A) low Li-Muscovite B) Li-muscovite C) 26837 lepidolite D) 28158 ppm lepidolite E) 28447 ppm lepidolite F) polylithionite (previous page).

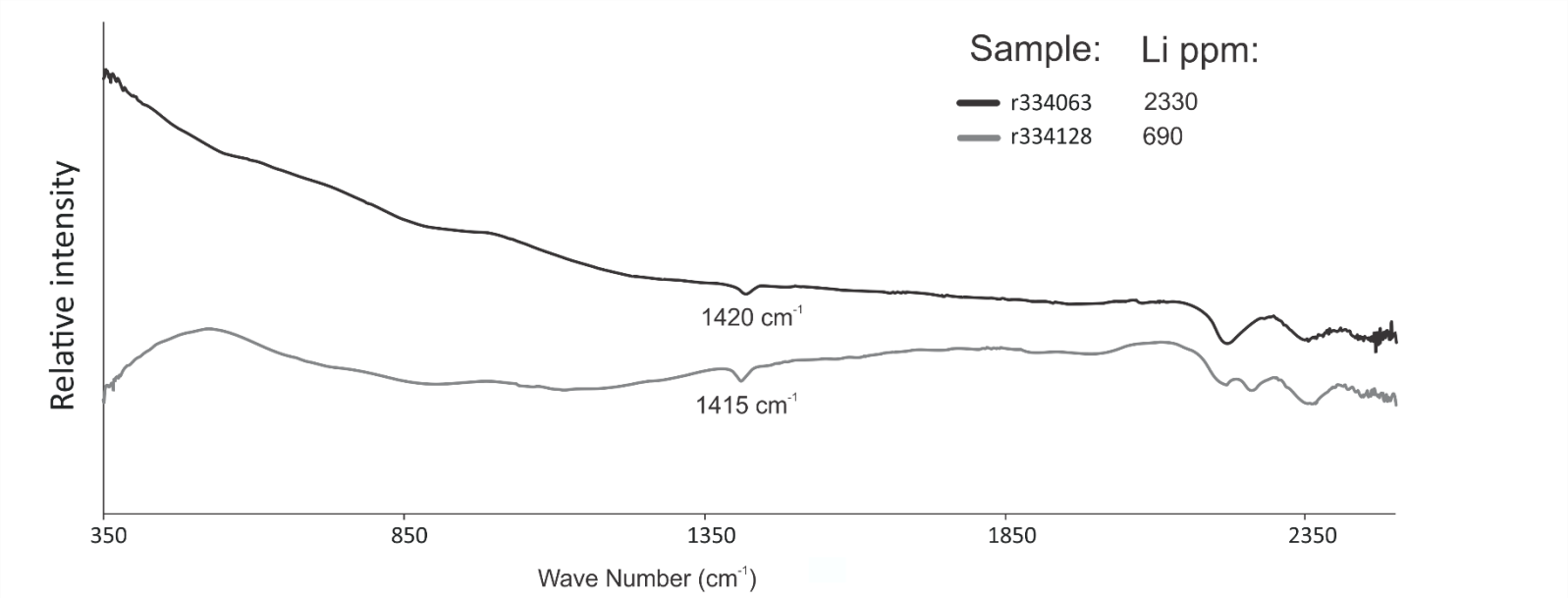

Figure 9: Spectra for 2 drill core samples from the contact of the Davis Lake Pluton with Meguma metawackes at the East Kemptville deposit, Nova Scotia.

4.1.2 Orientation

To determine whether grain orientation effects the infrared spectra of sheet silicates, infrared spectra were collected from the tetrahedral orientation (where the probe was oriented perpendicular to cleavage), and octahedral orientation (where the probe was oriented parallel to cleavage), of the same sample of muscovite. The position of absorption features for these two orientations of sample m10000 are depicted in Figure 10. There were 3 main observations:

1) A hull was observed in the spectrum from the octahedral orientation around 350-850 cm^{-1}. This is replaced a broad band in readings from the tetrahedral orientation.

2) The absorption features observed at 970 and 1411 cm^{-1} in the spectrum from the tetrahedral orientation are deeper than in the spectrum from the octahedral orientation.

3) Apart from the 970 and 1411 cm^{-1} features, absorption bands are consistent in position and intensity between the two orientations.

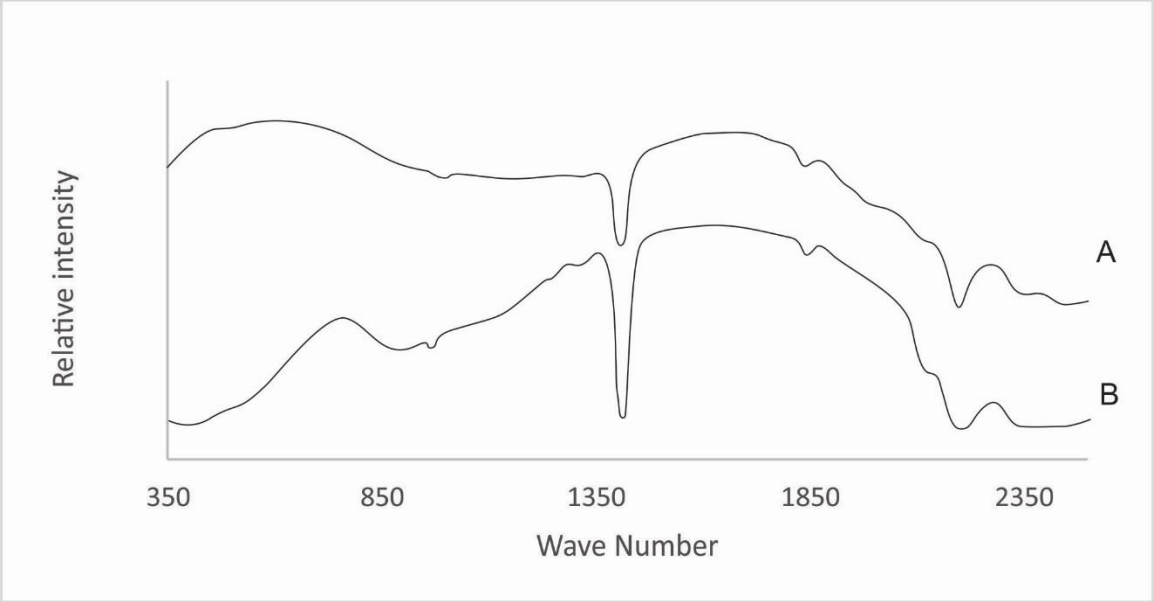

Figure 10: Orientation investigation of muscovite sample m10000 (explained in Figure 6) showing the spectral response of A) the octahedral layers stacked together, and B) the flat-lying tetrahedral layer.Absorption at 941cm^{-1} is observed in the tetrahedral orientation. This feature is not observed in the octahedral layers.

4.1.3 Treatment with molten lithium nitrate ($LiNO_3$) bath

To determine the effect of added Li to muscovite on the infrared response, spectra were collected at intervals of 72 and 240 hours of treatment with molten $LiNO_3$. For each time interval, a control sample of the same muscovite material was heated in a separate crucible at the same temperature in the absence of molten $LiNO_3$. Figure 11 shows the evolution of the spectra for the control and treated sample after each interval of treatment. To determine instrumental precision, multiple readings were taken for the 240 hour sample. Figure 12 shows the instrumental precision of readings on the sample after 240 hours of treatment. There were 5 main observations.

1) For all heated samples, intensity increases sharply around 500 cm^{-1}. This increase in intensity does not appear in the sample before heating.

2) After 72 hours of treatment, strong absorption was observed around 1931 cm^{-1}. However, this feature was no longer observed after 240 hours of treatment.

3) After 72 hours the relative absorptions at 2204 and 1414 cm^{-1} are deeper than the same features in the other samples.

4) Instrumental precision for the 240 hour sample is such that the position of all absorption features are reproducible from reading to reading. The intensity of absorption features however, vary slightly from reading to reading.

5) Absorption near 915cm^{-1} was not observed in any of the m10000 samples before or after treatment.

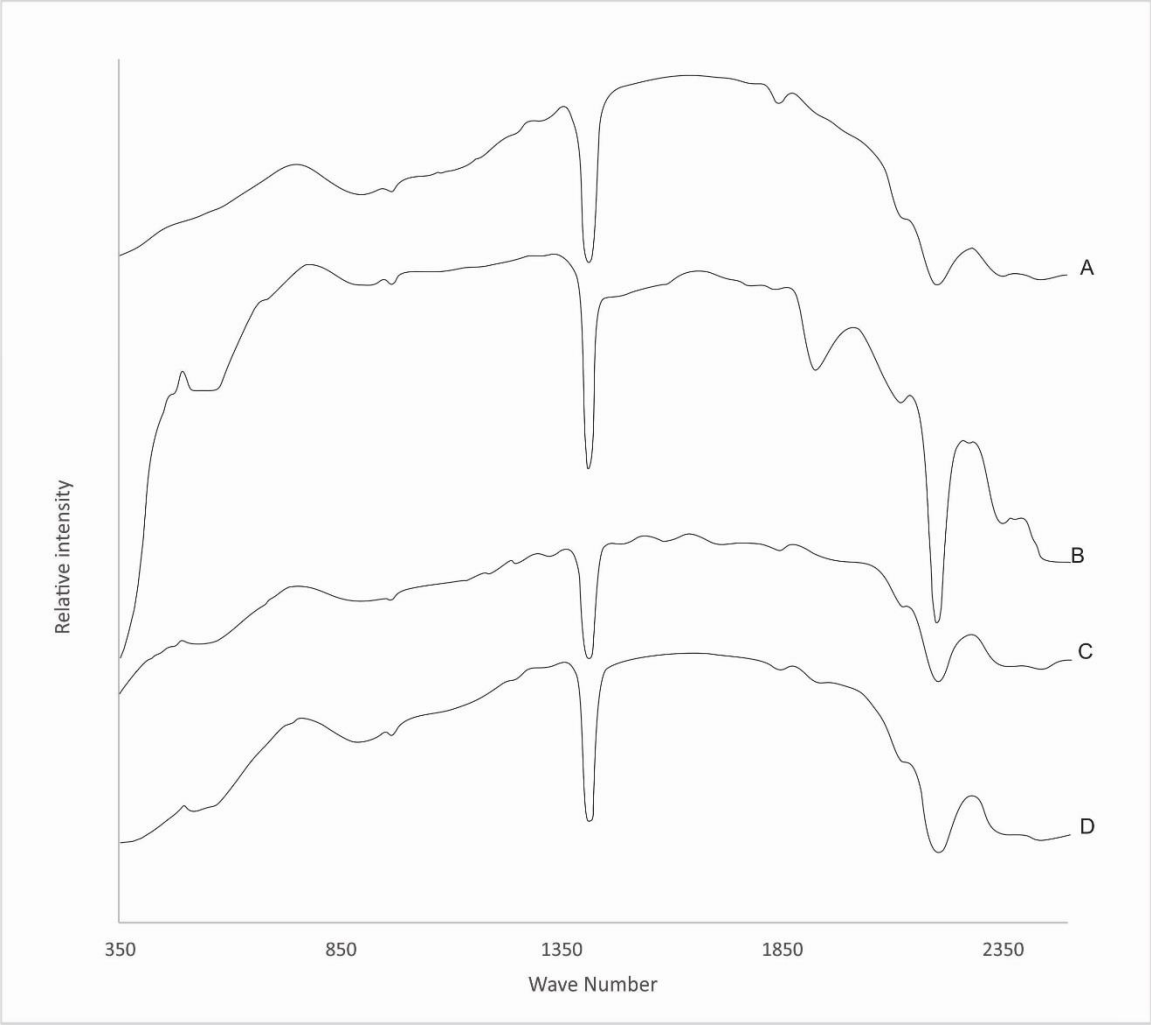

Figure 11: Infrared spectra of muscovite sample M10000 from the Li salt treatment experiments. A) before treatment and at room temperature, B) 72 and C) 240 hours of treatment with $LiNO_3$ at 300°C and finally, D) 240 hours at 300°C in the absence of molten LiNO3 (control).

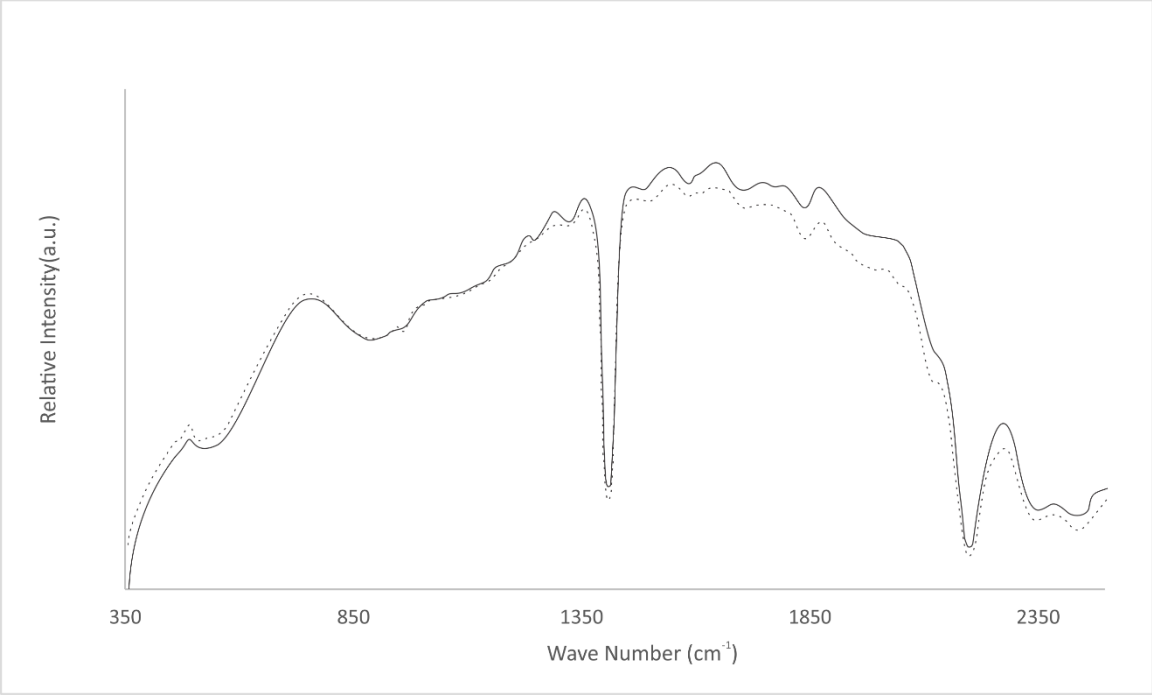

Figure 12: Duplicate of infrared readings of sample m10000 after 240 hours of treatment with molten $LiNO_3$ at 300°C to illustrate instrumental precision.

4.2 Laser ablation inductively coupled plasma mass spectrometry (LA-ICP-MS)

To determine the trace element composition of the 6 standard samples, they were analyzed with LA-ICP-MS. The major and trace element composition of the 6 standard samples is shown in Table 4. The sample of polylithionite, m55285, shows the highest Li concentration, as well as the lowest Al concentration.

4.3 Scanning electron microscopy

To quantify data from the LA-ICP-MS analysis, true Al_2O_3 values were determined using the scanning electron microscope.

Table 4: Summary of Li contents for 6 standard mica compositions determined by LA-ICP-MS. All values are averages of 10 analyses per sample.

sample number	mean Li ppm	s.d. (1 sigma)
M23374	28447	1780
M55285	32375	372
M29059	28158	905
M6317	1958	305
M31893	26837	1267
M10000	54	3

5.0 Discussion

The infrared absorption features of micas can be grouped into bands related to the OH stretching region (3550-3750 cm^{-1}) and the lattice vibration (<3550 cm^{-1}). In the lattice vibration region, features attributed to interlayer cations are found in the 50-400 cm^{-1} range. Cations in the octahedral layers influence absorption features in the 300-600 cm^{-1} range. Cations within the $Si(Al)O_4$ tetrahedra influence absorption features in the 700-1200 cm^{-1} range (Beran, 2002). Hydroxyl bending produces absorption near 1300cm^{-1} (Clark, 1999). Duke (1994), attributed absorption near 2200 to Al-OH bending, allowing for Al quantification in micas using IR spectroscopy. Most field spectrometers however, are limited to wave numbers in the lattice vibration region. This study used a spectrometer limited to the 350-2500 cm^{-1} range. Therefore, we limit our study to cations, mainly lithium, occupying octahedral positions, and those influencing the $Si(Al)O_4$ tetrahedra.

5.1 Li-mica standard spectra.

For the assignment of absorption bands to specific structural behaviors (e.g. stretching, vibration etc.), this study adheres to the recommendations of previous authors: "A reliable approach for discerning the origin of particular IR absorption bands is to combine theoretical considerations with empirical observations of phases having the same structure but differing in composition." (Beran, 2002).

5.1.1 Al-OH vibration region

The Al-OH band near 2200 cm^{-1} has been used in the past for Al quantification in micas (Duke, 1994). Their study attributed the decrease in wave-number from 2217 to 2199 cm^{-1} to Al replacement by Mg in muscovite. The Al-OH feature appears at a high frequency (2266cm^{-1}) in polylithionite sample m55285, reflecting its low Al concentration. M55285 also contains the highest concentration of Li. These results suggest that the high wavenumber of this Al-OH absorption band is related to the replacement of Al by Li.

5.1.2 SiO_2 bending region and tetrahedral cations

Bending of the SiO_2 bond in micas has been assigned to the 300-600 cm^{-1} region, and is known to be influenced by the cations occupying the octahedral positions of the mica structure (Beran, 2002). Cations able to occupy this position include Fe, Mg, Li, Mn, Zn, Al, Cr and Ti (Bishop et al., 2008). All samples analyzed, apart from m55285 show absorption from 563-584 cm^{-1}. These results suggest that the absorption bands seen in each sample are reflecting the presence of octahedral Al. Conversely, the lack of this feature in M55285 reflects its low Al concentration. The lack of absorption in in the SiO_2 region is further evidence to support the replacement of Al by Li in m55285.

5.2 Treatment with $LiNO_3$

With the exception of the 72 hour sample, absorption features in the spectrum of the muscovite sample before treatment with heat or molten $LiNO_3$ are consistent in terms of position and similar in terms of intensity. The large absorption feature near 1931 cm^{-1} in the 72 hour sample is likely an exaggeration of the small drop in intensity also seen in this position in the other samples. Similarly, the relatively high absorption at 2204 and 1414 cm^{-1} are also exaggerations of features found in the other samples. This exaggeration of intensity may be the result of improper calibration or more likely, sample thickness.

The reported (White et el., 1996) absorption feature near 915cm^{-1} was not observed in any of the m10000 samples before or after treatment. However, absorption near 970cm^{-1} was observed in all samples. Absorption near the 915 cm^{-1} region has been assigned to O-H… X^{3+} bending (Serratosa & Bradley, 1958) where X is any cation interacting with the O-H bond. Elimination of this feature after treatment with $LiNO_3$ has been assigned to Li entering empty octahedral sites reducing the bending frequency of O-H… X^{3+} (White et al., 1961). The study was unable to reproduce these findings. It is possible that the oxtahedral positions in the sample were already occupied prior to treatment, and therefore the bending of O-H… X^{3+} was already reduced, producing no absorption in the first spectra of the untreated sample.

5.3: Limitations

5.3.1 Limitations: calibration

To explain the difference in intensity of certain features it is necessary to understand the calibration process of the instrument. During IR measurements, the spectral response of

the sample is normalized to the spectral response of a reference material used during calibration. It is assumed that the standard used during calibration produce close to 100% reflectance. In this study a Spectralon puck attained from ASD was used as a reference during calibration. To reduce the effect of contamination during calibration, the Spectralon reference material was cleaned with compressed air before each calibration. Unfortunately, the Spectralon standard was lightly stained throughout the study in various physical locations. If the standard is slightly contaminated, the standard will produce less than 100% reflection, causing the spectral response of the sample to appear higher than the true value. The staining of the Spectralon standard may account for the difference of intensity of features at the same wavelength from sample to sample. This may also account for differences in intensity of some absorption features at the same wavelength for readings of the same sample, such as those in the instrumental precision portion of this study.

5.3.2 Limitations: sample thickness

Another explanation for these reflection/absorption intensity variations relates to sample thickness. Calculations of muscovite sample thickness have been attempted using the intensity of absorption features and the Beer–Lambert law. These studies rely on the fact that the intensity of an absorption feature for a given bond is directly proportional to the thickness of the sample (Busigny et al., 2003). At the 72 and 240 hour time increment, sheets were removed for infrared analysis and the remainder of the material was placed back into the furnace. The treated 72 hour sample, being only one muscovite sheet in thickness, was by far the thinnest sample. Therefore it is feasible that strong absorption band near 1931cm^{-1}, and the relatively less strong absorption bands near 2204 and 1414cm^{-1} are exaggerated due to sample thickness.

5.4 Orientation

It is generally understood that the orientation of samples during measurements does not effect the resultant spectra. For example, in a study quantifying NH_4 content in muscovite, infrared readings were taken at various angles perpendicular to the cleavage direction (Busigny et al., 2003). Absorption bands observed at different angles for the sample were consistent within instrumental error. Differences in intensity between the octahedral and tetrahedral orientation at 970 and 1411 cm^{-1} are likely due to the calibration error described in the previous section rather than orientation.

6.0 Conclusion

6.1 Main findings

1) Orientation does not effect the position of diagnostic features in micas. The relative intensity of features are explained by differences in calibration and sample thickness.

2) White reference quality and sample thickness influence the relative absorption, but not the position of features.

3) Al-OH absorption bands will shift to higher wave number as Al in octahedral sites is replaced. This relationship was seen in drill core samples from the East Kemptville deposit. Because Li replaces Al in lithium-micas such as polylithionite, Al-OH absorption at higher wave numbers may be used to infer higher end member polylithionite content, and therefore higher Li content.

4) No relationship was found between Li concentration and lack ofabsorption near 915cm^{-1}.

6.2 Recommendations

1) If the 915cm^{-1} feature does shrink in response to octahedral cations such as Li, it may be an important feature in Li-quantification using IR spectroscopy. For this reason, more work focusing on absorption in this region is recommended. Future experiments treating micas with Li salts should be conducted, ensuring that samples start with sufficient octahedral vacancies. At different and increasing duration of Li salt treatment, infrared and compositional data should be measured without removing sheets of mica from the book. This will ensure that changes in spectra are reflecting changes only in Li concentration.

2) The Al-OH absorption feature should be considered as a possible exploration indicator of Li in Lithium micas in which Al has been replaced by Li.

7.0 References

Allen, C. 2015. Exploratory work well underway at East Kemptville mine site. thevanguard, Yarmouth, Nova Scotia, (1 page web interview).

Beran, A. 2002. Infrared spectroscopy of micas. Reviews in Mineralogy and Geochemistry, 46: 351-369.

Bishop, J., Lane, M., Dyar, M., and Brown, A. 2008. Reflectance and emission spectroscopy study of four groups of phyllosilicates: Smectites, kaolinite-serpentines, chlorites and micas. Clay Minerals, 43: 35-54.

Busigny, V., Cartigny, P., Philippot, P., and Javoy, M. 2003. Ammonium quantification in muscovite by infrared spectroscopy. Chemical Geology, 198: 21-31.

Clark, R.N. 1999. Spectroscopy of rocks and minerals, and principles of spectroscopy. Manual of remote sensing, 3: 3-58.

Duke, E.F. 1994. Near infrared spectra of muscovite, Tschermak substitution, and metamorphic reaction progress: Implications for remote sensing. Geology, 22: 621-624.

Eugster, H.P. 1985. Granites and hydrothermal ore deposits: a geochemical framework. Mineralogical Magazine, 49: 7-23.

Gruber, P.W., Medina, P.A., Keoleian, G.A., Kesler, S.E., Everson, M.P., and Wallington, T.J. 2011. Global lithium availability. Journal of Industrial Ecology, 15: 760-775.

Halter, W.E., Williams-Jones, A.E., and Kontak, D.J. 1996. The role of greisenization in cassiterite precipitation at the East Kemptville tin deposit, Nova Scotia. Economic Geology, 91: 368-385.

Jaskula, B. 2016. Lithium. United States Geological Society, United States of America (1 page USGS report).

Jørgensen, P. 1964. Infrared Absorption of O---H Bonds in Some Micas and Other Phyllosilicates. Clays and Clay Minerals, 13: 263-273.

Kesler, S.E., Gruber, P.W., Medina, P.A., Keoleian, G.A., Everson, M.P., and Wallington, T.J. 2012. Global lithium resources: Relative importance of pegmatite, brine and other deposits. Ore Geology Reviews, 48: 55-69.

Kontak, D.J. 1990. The East Kemptville topaz–muscovite leucogranite, Nova Scotia I. Geological setting and whole rock geochemistry. Canadian Mineralogist, 28: 787-825.

Kontak, D.J., and Chatterjee, A.K. 1992. The East Kemptville tin deposit, Yarmouth County, Nova Scotia: a Pb-isotope study of the leucogranite and mineralized greisens—evidence for a 366 Ma metallogenic event. Canadian Journal of Earth Sciences, 29: 1180-1196.

Kontak, D.J., and Dostal, J. 1992. The East Kemptville tin deposit, Yarmouth County, southwestern Nova Scotia: a lithogeochemical study of the wallrock metasedimentary rocks. Atlantic Geology, 28: 63-83.

Kontak, D., Mulja, T., and Hingston, R. 1986. The East Kemptville Sn deposit: preliminary results from recent mapping. Tenth Annual Open House and Review of Activities.Nova Scotia Department Mines & Energy, Information Series, no. 12 p. 97-103.

Muecke, G., Elias, P., and Reynolds, P. 1988. Hercynian/Alleghanian overprinting of an Acadian terrane: 40Ar/39Ar studies in the Meguma zone, Nova Scotia, Canada. Chemical Geology: Isotope Geoscience section, 73: 153-167.

Robert, J., Bény, J.M., Beny, C., and Volfinger, M. 1989. Characterization of lepidolites by Raman and infrared spectrometries. I. Relationships between OH-stretching wavenumbers and composition. Canadian Mineralogist, 27: 225-235.

Sedge, C. 2015. Characterizing the mineral domains of Li-(Rb-Cs) enrichment at the East Kemptville Sn-(Cu-Zn-Ag) deposit, southwestern Nova Scotia. Knowledge Transfer Report to Avalon Rare Metal Inc. from Saint Mary's University, Halifax, Nova Scotia, 1-34.

Serratosa, J.M., and Bradley, W. 1958. Infra-red absorption of OH bonds in micas. Nature, 181: 111.

Sinclair, W.D. 1996. Vein stockwork tin-tungsten. In Geology of Canadian Mineral Deposit Types Edited byGeological Survey of Canada, pp. 409-410-420.

Tindle, A.G., and Webb, P.C. 1990. Estimation of lithium contents in trioctahedral micas using microprobe data: application to micas from granitic rocks. European Journal of Mineralogy, 595-610.

Tischendorf, G., Förster, H., and Gottesmann, B. 1999. The correlation between lithium and magnesium in trioctahedral micas: Improved equations for Li2O estimation from MgO data. Mineralogical Magazine, 63: 57-74.

Tischendorf, G., Gottesmann, B., Foerster, H., and Trumbull, R.B. 1997. On Li-bearing micas: estimating Li from electron microprobe analyses and an improved diagram for graphical representation. Mineralogical Magazine, 61: 809-834.

White, J.L., Bailey, G., Brown, C., and Alrichs, J. 1961. Infra-red investigation of the migration of lithium ions into empty octahedral sites in muscovite and montmorillonite. Nature, 190: 342-342.